Journal of Materials Chemistry A

Accepted Manuscript

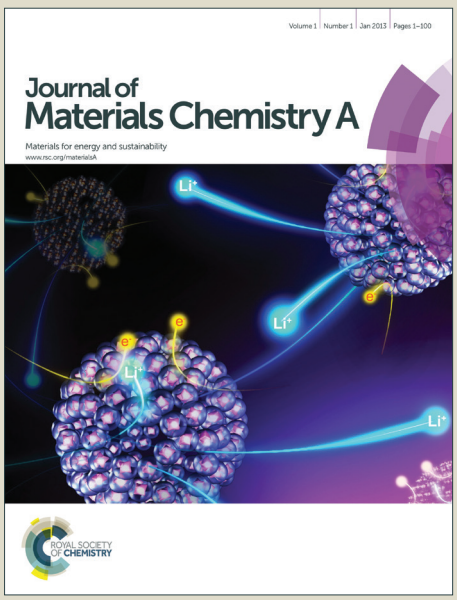

ROYAL SOCIETY OF CHEMISTRY

www.rsc.org/materialsA

Facile Synthesis of Ge@FLG Composites by Plasma Assisted Ball Milling for Lithium Ion Battery Anodes

Liuzhang Ouyang[a,b], Lina Guo[a,b], Weihua Cai[c], Jianshan Ye[c], Renzong Hu[a,b], Jiangwen Liu[a,b], Lichun Yang[a,b], Min Zhu[a,b]*

[a]School of Materials Science and Engineering, South China University of Technology, Guangzhou, 510641, People's Republic of China

[b]Key Laboratory of Advanced Energy Storage Materials of Guangdong Province, South China University of Technology, Guangzhou, 510641, People's Republic of China

[c]School of Chemistry and Chemical Engineering, South China University of Technology, Guangzhou, 510641, People's Republic of China

ABSTRACT: Efficient production of graphene or its germanium (Ge) composites remains a challenge, although Ge nanoparticles (NPs) wrapped with graphene are suitable for preventing the large volume change of anodes for lithium ion batteries during Li uptake and release processes. This work is the first simple, efficient in situ synthesis of excellent structure of Ge NPs wrapped with few-layer graphene sheets (abbreviated as Ge@FLG) from commercial Ge powders and natural graphite by one-step ball-milling process assisted by dielectric-barrier discharge plasma. Because of their unique structure, Ge@FLG electrodes exhibit better electrical conductivity, low initial capacity loss, good cycling capability, and rate resilience compared with Ge@C electrodes prepared by conventional milling. This work highlights a new method for the efficient production of Ge@FLG composites and their applications in lithium ion batteries and in other technologies.

KEYWORDS: Germanium ·few layer graphene sheets ·lithium ion batteries ·dielectric-barrier discharge plasma

*Corresponding author. Tel.: +86-20-87113924; fax: +86-20-87111317
E-mail address: memzhu@scut.edu.cn

1. Introduction

With the large demand for high-energy-density lithium ion batteries (LIBs) in essential applications such as portable electronics, electric vehicles, and aerospace carriers, high-capacity anode materials are now replacing commercial graphite anodes with limited theoretical specific capacity (372mAh g^{-1}).[1–3] The Group IV materials (Si, Ge, and Sn) $Li_{4.4}Si$, $Li_{4.4}Ge$, and $Li_{4.4}Sn$ have drawn much attention because of their high theoretical capacities (4200,1600, and 990 mAh g^{-1}, respectively).[2] Among the above-mentioned most important three anode materials, Ge possesses unique merits in having electrical conductivity and capacity that are higher than those of Sn. In particular, the diffusion rate of Li^+ in Ge is about 400 times greater than that in Si at room temperature,[4] corresponding to high charge and discharge rates. However, Ge electrodes still suffer from the following problems: They have poor cycling stability mainly because of their large volume changes (370%) during lithiation and delithiation, leading to cracking and pulverization of electrodes.[5] They incur serious initial capacity loss due to formation of a film of solid electrolyte interphase (SEI). Lastly pure Ge has a high cost.

There are some common ways to solve these problems, such as the use of nanosized Ge, three-dimensional porous structures,[6] combining Ge with other inert materials, and coating it with carbon or graphene. Among these strategies, combining Ge nanoparticles (NPs) with graphene sheets is the most attractive, as graphene can enhance the cycling stability and rate capability of Ge electrodes. Graphene sheets have unique properties such as excellent electrical and thermal conductivities, large specific surface area, high mechanical strength, and inherent flexibility. They may be used as buffer material and highly conductive network for the entireelectrode.[7–12] Xue et al.[9] mixed Ge@C NPs with reduced graphene oxide (RGO) through a chemical method to obtain Ge@C/RGO, which contained 58.3wt % Ge. Ge@C/RGO electrodes had 52% capacity retention (940 mA h g^{-1}) after 50cycles at 50 mA h^{-1} relative to the initial value, 1803mAhg^{-1}. Kim et al.[12] prepared graphene/Ge nanowires (NWs) by growing graphene on a Ge NW surface through chemical vapor deposition (CVD). The electrodes, which contained

98.3wt % Ge, maintained 1059mAhg^{-1} after 200 cycles (90% retention) at 4.8Ag^{-1}. These two recent examples show that the performance of Ge electrodes was markedly improved by these methods. However, the synthesis of Ge@graphene nanocomposites is still constrained to complex chemical processes or CVD, which are expensive and have low production coefficients. These methods also release pollutants and pose difficulties in commercial utilization.[13–16] However, the initial capacity loss is still too high to improve the conductivity of the electrode; the diffusion rate of Li^+ and further reaction of the electrolyte may affect the kinetics of Li^+ release and uptake and the stability of the entire cell.

Given these achievements, the key issue is the development of a simple and economical synthesis method of Ge@graphene with controlled nanostructure that enables high electrochemical performance and mass production and reduces the initial capacity loss. In the present study, milling assisted by dielectric-barrier discharge plasma (P-milling) was used to address this problem. With this method, Ge NPs dispersed in few-layer (about 10 layers) graphene sheets (Ge@FLG) were synthesized from commercial Ge and graphite in one step. These NPs enabled high performance of anodes in LIBs. It also provides a new route for practical applications of Ge-based anode materials for LIBs.

2. Experimental

Preparation of Ge-C and Ge@FLG composites

To examine thoroughly the contributions of the P-milling process to the formation of Ge@FLG, we prepared two counterparts of the one-step insitu synthesized Ge@FLG nanocomposite by P-milling of commercial Ge powders and graphite powders (abbreviated as P-milling Ge/C). Ge powders and graphite processed by conventional ball milling (abbreviated as C-milling Ge/C) were used to analyze the effects of conventional ball milling without DBDP on the morphology and performance of the material. For comparison, a third experiment was carried out to examine the effect of Ge particles size and carbon resources, in which Ge powders were pre-milled for 5h to

nano-size and expandable graphite (EG) was high-temperature treated (abbreviated as P-milling Ge5h/EG). What needs to be emphasized is that, to avoid the influence of components ratios on the microstructure, the loading mass of Ge in all the three Ge-C composites is 50%.

The two P-milling nanocomposites were prepared through the following procedures. For the first nanocomposite, commercial germanium powders (98%,≤5 μm) and graphite powders were combined at a mass ratio of 1:1. The ball-to-powder ratio was 50:1.The mixtures were exposed to DBDP in the mill vial, which contained two electrodes. As in our previous work, a vibration-type ball mill was used. The milling cylinder vibrated with a double-amplitude of 7 mm and a frequency of 24 Hz. Before the milling process, the vial was evacuated and then backfilled with high-purity argon (0.11–0.12Mpa). The powder mixtures were milled for 10 h, according to an earlier work. After 10 h the powders began to aggregate, leading to deteriorated performance. For the second nanocomposite, Ge powders were P-milled for 5h in the same manner as above. EG was heated in a tube furnace at 1000 °C for half an hour to obtain wormlike EG. The preprocessed Ge powders and EG were combined in a mill vial for P-milling with the same parameters as above. For comparison, conventional milling was also used to prepare Ge/C powder mixtures with 1:1 mass ratio and 50:1ball-to-powder ratio. The powders were milled for 10 h under an argon atmosphere by using the same milling methods but without DBDP.

Characteration

The morphology and composition of the materials prepared by C-milling and P-milling were characterized by using a Philips X'Pert MPD X-ray diffractometer with Cu Kα radiation, a Nano430 scanning electron microscope, a JEM-2100 transmission electron microscope, and a LabRaMaramls Raman spectrophotometer.

Electrochemical measurements

Electrodes for testing consisted of 80wt% active powder material, 10wt% acetylene black (conducting agent), and 10wt% polyvinylidene fluoride dissolved in *N*-methyl pyrrolidinone (binder). These components were mixed

by a magnetic stirrer to form slurry and then coated onto copper foil. After drying at 120 °C for 12 h under vacuum, they were pressed and cut into a suitable size for the assembly of CR2016 coin-type half cells in an argon-filled glove box with lithium ribbons as counter electrodes. The separator was polyethylene membrane (Teklon@Gold LP) and the electrolyte was 1M $LiPF_6$ in ethylene carbonate/diethylene carbonate/ethyl methyl carbonate solution (1:1:1, v/v/v) (Guangzhou Tinci High-Tech Material Co.Ltd.). Cycling performance tests were galvanostatically implemented on an Arbin BT-2000 at various charge and discharge current densities and voltage range of 0–1.5V (versus Li/Li^+).

3. Results and discussion

The X-ray diffraction (XRD) patterns in Figure 1 suggest small amounts of GeO_2 in the C-milling Ge/C and P-milling Ge/C samples. Although the three samples were from the same commercial Ge source, there are no GeO_2 peaks in the XRD patterns of P-milling Ge5h/EG. The P-milling process might have purified the commercial Ge powders after size reduction through the P-milling preprocess. The contrast between pristine commercial Ge powders and previously P-milled high-purity and nanoscale Ge powders could be observed in the formation of Ge@FLG during the P-milling process. The XRD peak for carbon in the C-milling sample is much weaker than those of the two other P-milling samples, indicating the lower crystallinity or greater extent of degradation of carbon. Premilling of commercial Ge powders for 5h in the P-milling Ge5h/EG sample contributed to finer particles, as can be inferred from the wider peaks of Ge. The peaks of GeO_2 weakened markedly possibly because of its nanocrystallization and amorphization. Raman spectra (Figure 1) can help prove the formation of FLG in P-milling Ge/C and P-milling Ge5h/EG samples. Peaks at about 1350, 1580, and 2700cm^{-1} correspond to the typical D, G, and 2D (also known as G′) bands for carbon materials. The D peak indicates the existence of defects in sp^2 carbon material, the G band is related to the doubly degenerate zone center E_{2g} mode, and the 2D band represents the second order of zone-boundary phonons. The two samples of P-milling produced 2D bands that are

significantly different from those of the C-milling sample, indicating the presence of FLG.[17–19] The intensity ratio of band D and G I(D)/I(G) increased with the number of defects, as can be seen in the samples of C-milling (I(D)/I(G)>1.5), indicating more disordered carbon, in contrast to the ratio of the other samples (I(D)/I(G) <0.5). The I(G)/I(2D) ratio varied inversely with number of graphene layers. Raman spectra in Figure 1 show remarkable differences between P-milling and C-milling samples. However, the two P-milling samples were not significantly different. Thus, the outcome of P-milling Ge@FLG is independent of the size and purity of Ge powders and graphite source. In the unique structure of Ge@FLG, GeNPs are tightly wrapped with FLG sheets formed insitu, as also evidenced by scanning electron microscopy observations.

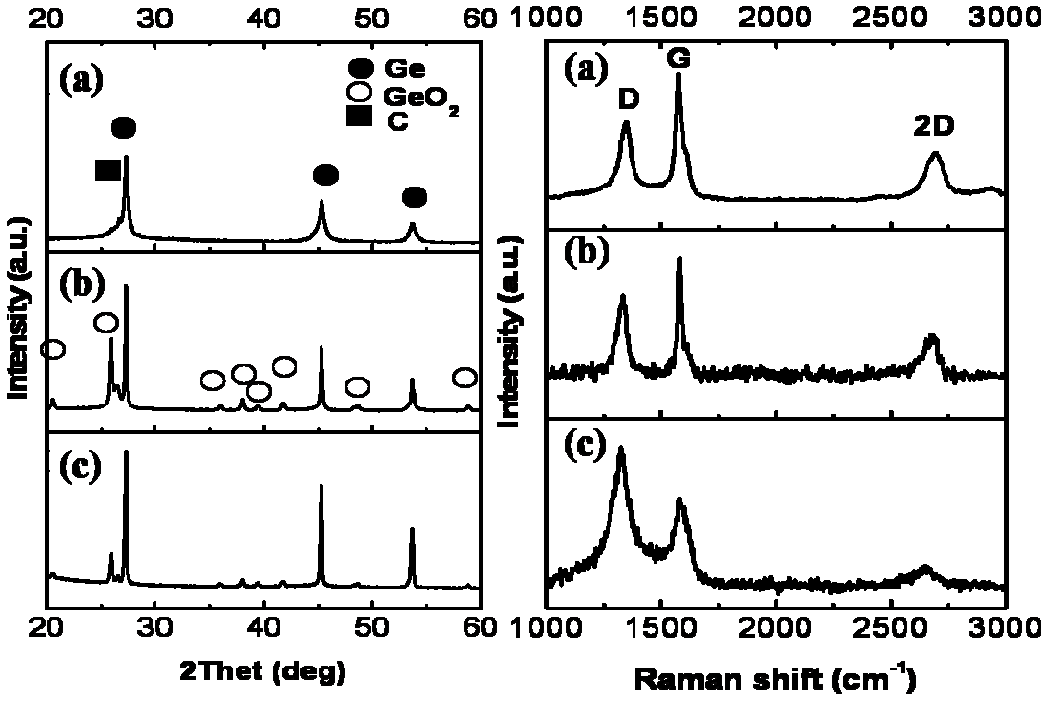

Figure1. XRD patterns, Raman shift spectra (514nm) for the three samples of (a) C-milling Ge/C. (b) P-milling Ge/C. (c) P-milling Ge5h/EG.

Figure 2 shows that the commercial Ge powders had a mean particle size of 3–4 μm (left bottom inset, Figure 2a). Its size was reduced to about 150–300nm after P-milling for 5h. The microstructure of NPs dispersed in cotton like carbon in the C-milling Ge/C sample was obtained (Figure 2b). In Figure 2c and d presented the back scattered electron images for the Ge@FLG, in which the bright particles are Ge nanoparticles and the gauze-like structure is from few-layer graphene sheets. And the structure of Ge NPs (average size about 150–300nm) of both samples wrapped with FLG sheets (10 layers) prepared by P-milling can be clearly seen indicating the same final Ge@FLG structure which is in accordance with their Raman spectra. This suggests that the Ge@FLG nanocomposites could be mechanically prepared in one step from commercial Ge and graphite powders.

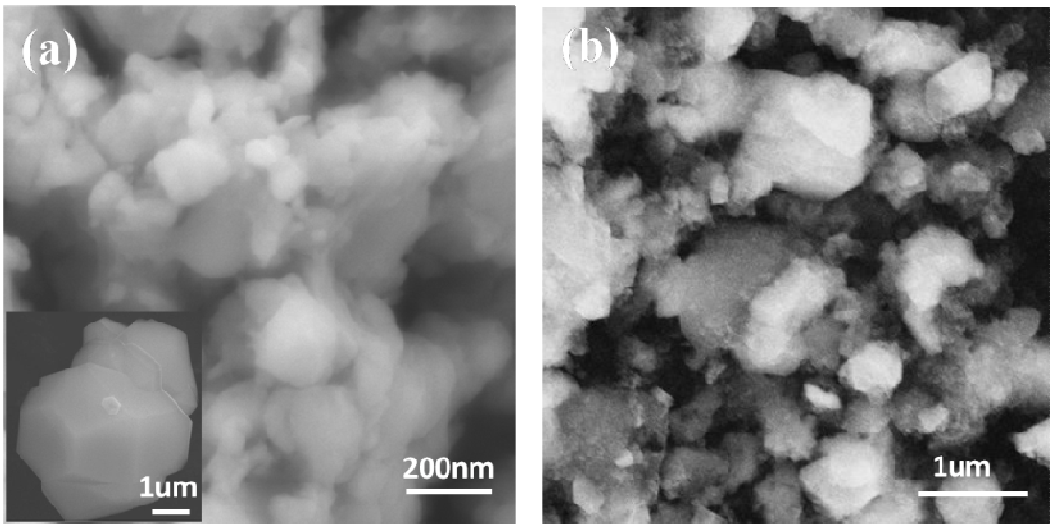

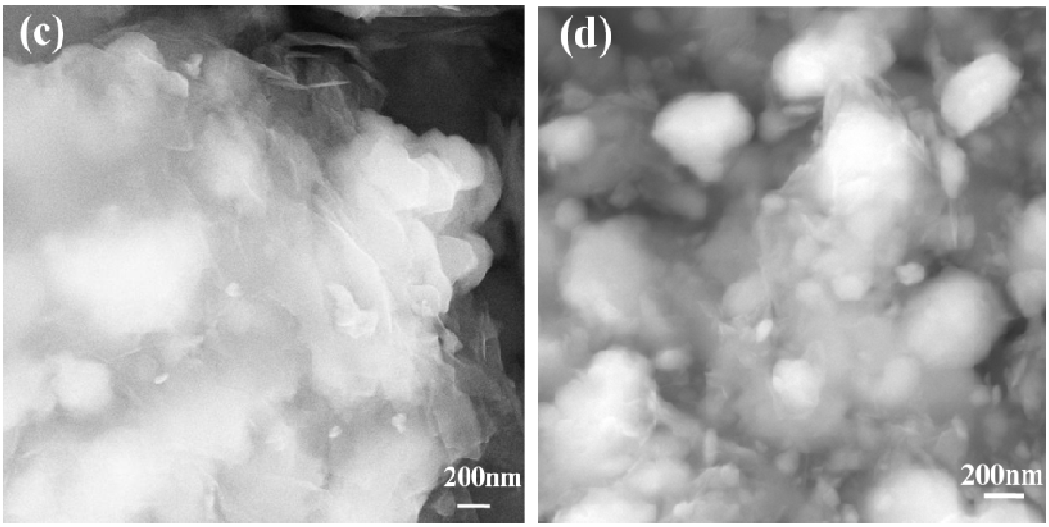

Figure2. SEM images of (a) commercial Ge powders (left bottom inset) and that after P-milling for 5h, (b) C-milling Ge/C, (c) P-milling Ge /C, (d) P-milling Ge5h/EG;

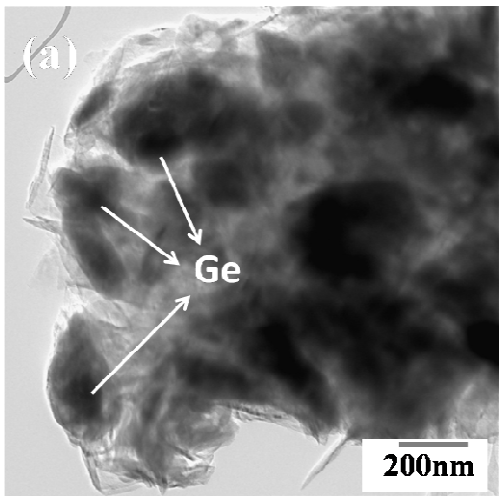

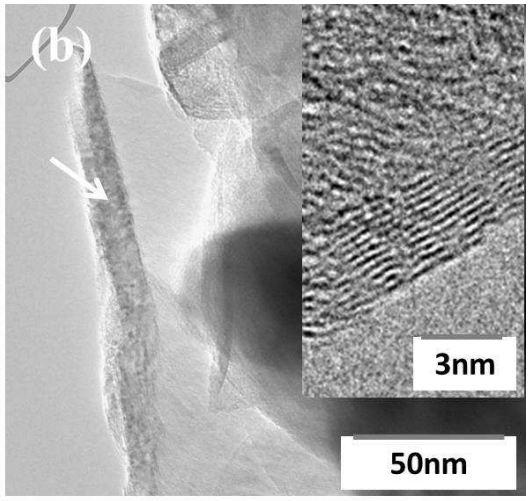

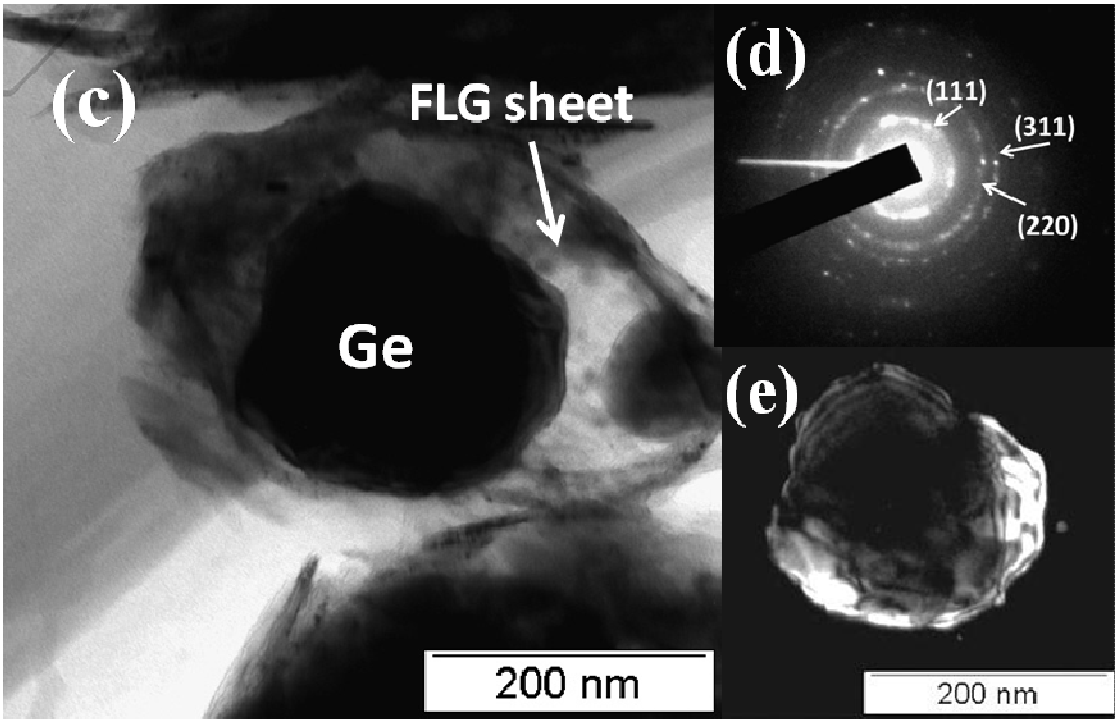

Figure3. (a), (b), (c) Bright field images of Ge@FLG microstructure for the as-prepared sample of P-milling Ge5h/EG and HR-TEM image of FLG sheet as inerted into image (b). (d) Selected area electron diffraction pattern of Ge particle. (e) Dark field image of a single Ge particle.

The microstructure of Ge@FLG composite was further investigated by transmission electron microscopy (TEM). Results for P-milling Ge5h/EG are shown in Figure 3a–d. Figure 3a shows that GeNPs were wrapped with FLG sheets, and that the wrapped structure was uniformly dispersed with the excess FLG sheets. In this structure, the FLG sheets had two protective roles. Figure 3b presents the magnified edges of the outer graphene sheet. The high-resolution TEM image on the left side shows that the FLG sheet was about 10 layers in thick, which is consistent with the Raman spectra of the two P-milling samples. Figure 3c shows the characteristic structure of Ge@FLG in which GeNPs of ~150nm size are tightly wrapped with FLG sheets. The selected area electron diffraction pattern and dark-field image of typical Ge NPs are presented in Figure 3d and e, respectively. The equal thickness fringes of Ge in Figure 3e suggested that there is no skill facet on the surface of smooth globular Ge

nanoparticle.

The formation mechanism of composites of Ge@FLG structure from Ge powders and nature graphite when treated by P-milling was investigated. Firstly, P-milling is an inexpensive, facile, green, controllable, and productive method. It was developed by combining dielectric-barrier discharge plasma (DBDP) with ball milling.[20,21] DBDP, a high-energy field far from equilibrium, can provide high-energy electrons that can lead to generation of atoms, radicals and excited particles.[22] Construction of unique nanostructures is facilitated by the synergetic effect of mechanical milling and DBDP. In the experiment, powders of Ge and graphite were sealed together with steel balls and pure argon (the dielectric medium) in a cylinder. Plasma, electrons, and ions were generated by gas ionization inside the cylinder. Ge powders underwent particle size reduction under the stress of the ball milling process. They cracked and even exploded because of rapid heating and acquired an activated surface because of the excited plasma. Secondly, under these conditions, graphite could split along the (0001) plane because the binding forces (van der Waals forces) between graphite layers are weak. Thermal explosion due to plasma heating can disrupt the binding force with the help of Ge NPs moving at high speed.[23, 24] Thus, graphene platelet sheets in a few layers were produced. Lastly, in continuous P-milling, Ge NPs were dispersed inside the loose FLG, and FLG was subsequently wrapped around GeNPs instantaneously. It is worth mentioning that this synthetic method can produce materials at kilogram scale and is amenable to upscale to massive production as shown in Figure 4. Most importantly, the Ge@FLG composite prepared through the P-milling process is a promising material for LIB anodes. The good cycling ability and rate capability of the electrodes could be proved in tests, as described below.

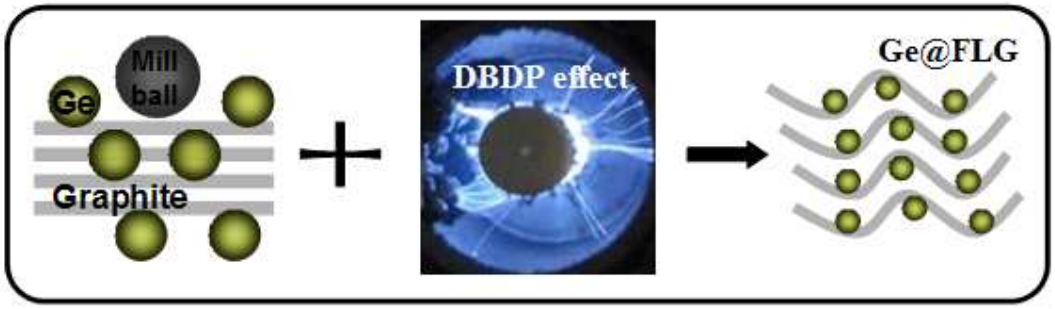

Figure4. Schematic illustration of the in-situ synthesis process of Ge@FLG nanocomposites by P-milling

The electrochemical performances of the C-milling Ge/C, P-milling Ge/C, and P-milling Ge5h/EG samples as anodes for LIBs were studied by galvanostatic cycling in the potential range of 0 to 1.5mV. 2016-Type coin cells were used, with the as-prepared materials as the working electrode and Li foil as the counter electrode. The discharge and charge files of the three electrodes in the first cycle at a low rate (0.05C) are shown in Figure 5a. The first discharge capacity of the C-milling Ge/C electrode was 2151.5mAhg^{-1} and its charge capacity was 979.8mAhg^{-1}, resulting in a low coulombic efficiency (45.5%). The irreversible capacity in the first cycle was partly because the decomposition of electrolyte and SEI formation. Another reason was due to the amorphous graphite and the existence of GeO_2 which consume Li^+ to generate Ge and Li_2O leading to more irreversible capacity loss. The first discharge and charge capacities of the P-milling Ge/C sample were 2081.8 and 1213.8 mAhg^{-1}, respectively, and those of the P-milling Ge5h/EG sample were 1480 and 991mAhg^{-1}, respectively; their coulombic efficiencies were 61% and 67%, respectively. The C-milling Ge/C electrode possessed the highest discharge capacity and lowest coulombic efficiency, and the P-milling Ge5h/EG electrode had the highest coulombic efficiency, indicating the improved reversible capacity of the first cycle, though there was still irreversible capacity loss because of the inherent characteristic of the electrode and the carbonic material. Apparently, the P-milling Ge5h/EG electrode had the lowest first-discharge capacity but close to the theoretical

capacity presenting the highest coulombic efficiency due to the high quality of the few-layer graphene and purified nano-Ge in the Ge@FLG structure. The C-milling Ge/C and P-milling Ge/C samples had much higher capacities, which are far beyond their theoretical capacity in the first cycle. This difference suggests that preprocessing of nanosized of Ge powders and heat treatment of graphite before P-milling could decrease the micro-defects and the irreversible capacity loss in the first cycle. During discharge, there were three voltage plateaus (at around 0.8, 0.6, and 0.3V) with C-milling Ge/C and P-milling Ge/C electrodes, two with P-milling Ge5h/EG electrode (at 0.8 and 0.3V). These correspond to the formation of a SEI and the lithiation of carbon or graphene at around 0.8V, as well as the reduction of GeO_2 to Ge at ~0.6V and ~0.3V in the Li–Ge alloying process.[25–27] The absence of a reduction voltage at 0.6V for P-milling Ge5h/EG confirms that P-milling could purify commercial Ge powders, and agrees with the XRD patterns. Figure 5b presents the cycling performance of the three electrodes at 0.4C.The rapid recession of cycles before the 10th cycle of the C-milling Ge/C and P-milling Ge/C electrodes maybe attributed to the reaction between Li and native GeO_2 and other defects.[28] The two Ge@FLG electrodes prepared by P-milling exhibited higher specific capacity and better cycling stability (769.5 and 846.3mAhg^{-1} after 50 cycles) compared with the C-milling Ge/C electrode (541.8mAhg^{-1}). Although the theoretical capacity of the three electrodes we prepared (Ge: C, 1:1, w/w) was 986mAhg^{-1}, the P-milling Ge5h/EG electrode had the highest capacity retention (86%) and that of the P-milling Ge/C electrode was 78%, both higher than that of the C-milling Ge/C electrode (55%). The cycling stability apparently benefitted from the unique structure of the Ge@FLG composite. It is hypothesized that the two graphene sheet in such structure alleviate volume changes of Ge NPs during the lithiation/delithiation process and that the active Ge materials with inner wrapped FLG sheets function as a coriaceous wall. Furthermore, the abundant FLG sheets can enhance the electric conductivity, high surface area, and ion diffusion rate. The rate capability performance (Figure 5c) suggests that at low rate (<1C), the C-milling Ge/C electrode possessed lower capability and poorer recovery after cycling at high rates. However, the electrodes

of P-milling Ge/C and P-milling Ge5h/EG not only exhibited good performance at a rate of 7.5C, but were also highly resilient. After 50 cycles and high-rate tests, the specific capacities at low rate could be restored to the initial values. Their high reversibility maybe attributed to the protection of the two tough FLG sheets synthesized insitu through the P-milling process, which had effectively avoided structural damage and pulverization of Ge NPs when large volume changes happened during the cycles.

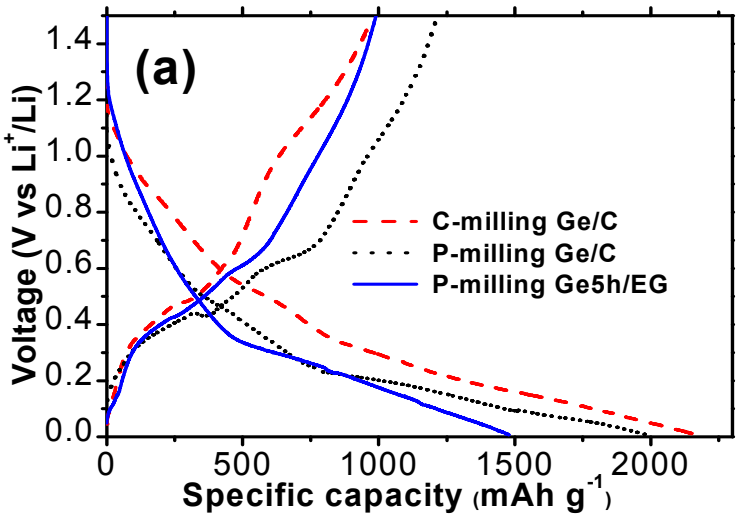

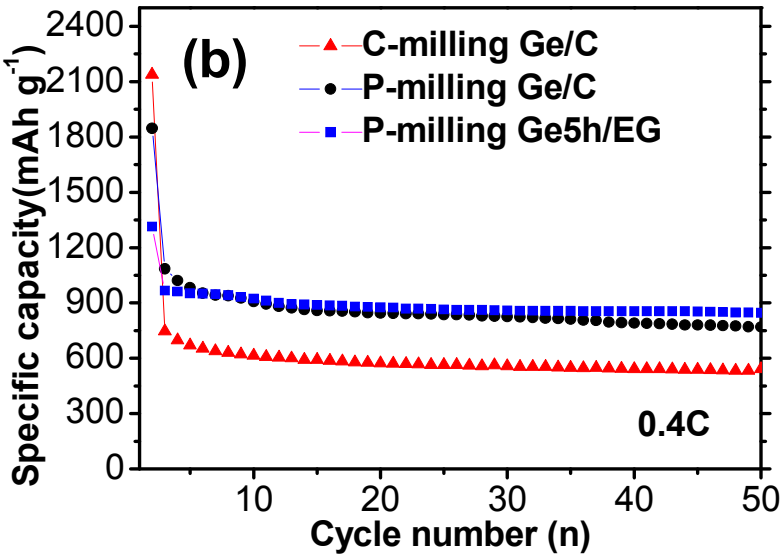

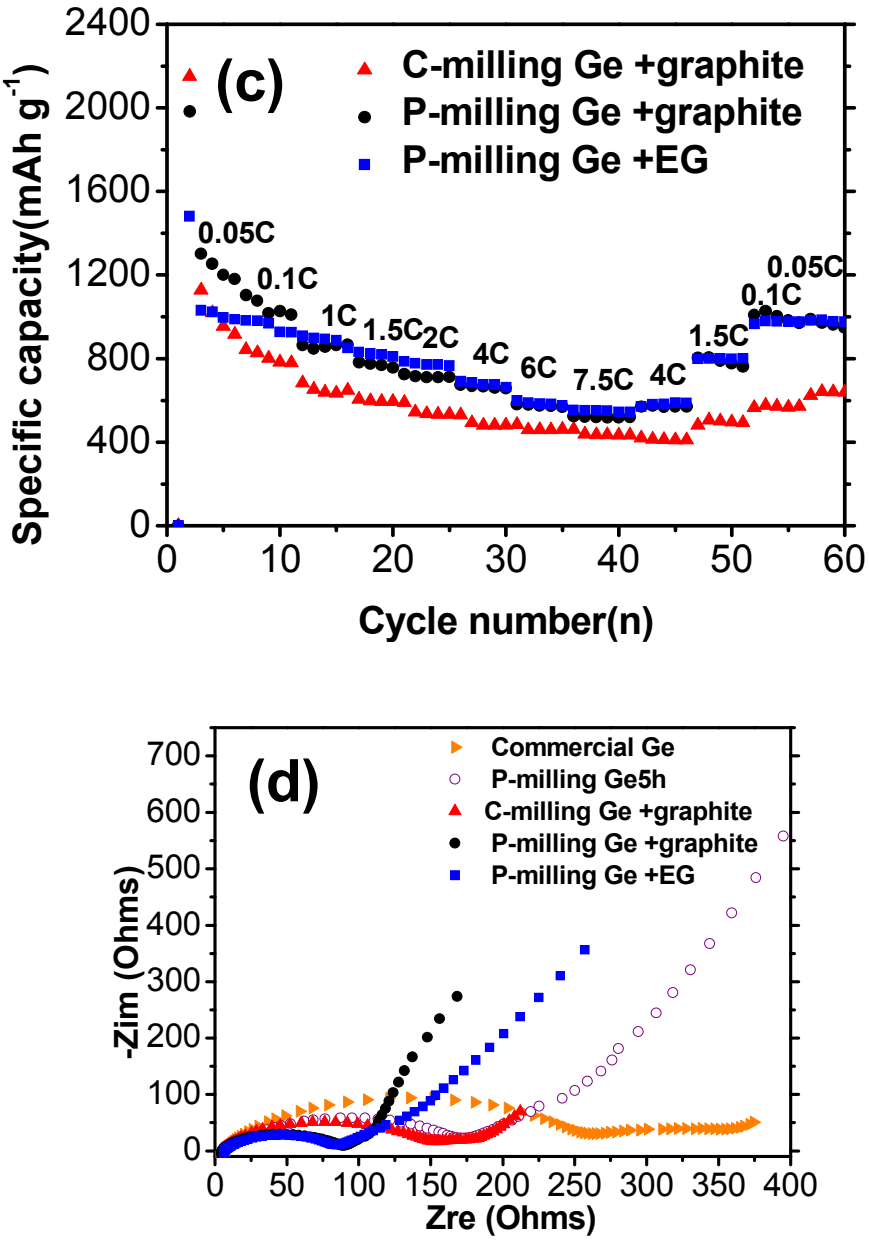

Figure5. (a) Galvanostatic discharge and charge files of the electrodes of C-milling Ge/C, P-milling Ge /C, P-milling Ge5h/EG in the first cycle at 0.05C (50mA/g). (b) Cycle performances of the electrodes at 0.4C (200mA/g). (c) Rate performances of the electrodes. (d) Nyquist plots of the as-prepared electrodes of the electrolytes (1.5V *vs* Li^+/Li).

The cycling ability and rate capability of the electrodes might also be related to their charge-transfer process. The electrical conductivity of the P-milling electrodes was greatly enhanced, as evaluated by electrochemical impedance spectroscopy (1.5V vs Li^+/Li). Figure 5d compares Nyquist plots for commercial Ge powder, the sample subjected to P-milling for 5h, as well as C-milling Ge/C, P-milling Ge/C, and P-milling Ge5h/EG samples. Impedance spectra (curves in Figure 5d) may be analyzed by examining the semicircle in the middle-frequency region, which is associated to the charge-transfer resistance of the electrode/electrolyte interface.[28, 29] The electrode constructed from commercial Ge powder produced the largest semicircle, and the P-milling Ge electrode produced a smaller one. This difference suggests that the conductivity was improved because of the decrease in Ge particle size and because of activation of the particle surface through the P-milling process. Remarkably, curves of the P-milling Ge/C and P-milling Ge5h/EG samples had almost the same semicircle radii (~90Ω), which are much smaller than those of the curves for the C-milling Ge/C and pure Ge electrodes, indicating that P-milling of Ge with graphite led to a very low charge-transfer resistance. Significant improvement of the conductivity of the P-milling Ge/C and P-milling Ge5h/EG electrodes at ~90Ω is apparently related to the unique structure of Ge@FLG. In such structure, Ge NPs surround FLG and enhance the electron flow.

4. Conclusions

In conclusion, we have demonstrated for the first time the great advantages of P-milling in the preparation of a Ge@FLG nanocomposite anode for LIBs that has high capacity, high conductivity, high capacity rate, less initial capacity loss and stable cycling ability. This nanocomposite has the unique structure of Ge NPs (150nm) tightly wrapped with FLG sheets (10 layers) that are dispersed homogenously in the FLG matrix. Thus, the structure has high stability because of the protective buffer of two levels of FLG. Furthermore, one-step synthesis from raw material avoids contamination and results in a uniformly dispersed structure, which in turn reduces the initial

capacity loss and enhances electrical conductivity. The Ge@FLG nanocomposite prepared by P-milling process anodes affords lower charge-transfer resistance (~90Ω) because of the high stability and conductivity of the structure, which cannot be achieved through the conventional milling method. A capacity of 846.3mAhg^{-1} and retention of 86% of the Ge@FLG nanocomposite (P-milling Ge5h/EG sample) containing 50wt % Ge could be retained after 50 charge/discharge cycles at a rate of 0.4C, with 67% initial reverse capacity. Thus, this work provided an efficient way to simultaneously solve the challenging problems of achieving stable high capacity and mass production of Ge@FLG nanocomposite anode through P-milling.

Conflict of interest: The authors declare no competing financial interest.

Acknowledgements

This work was financially supported by the National Natural Science Foundation of China (Nos. 51201065, U1201241, 51271078 and 51231003), the Natural Science Foundation of Guangdong Province (No. S2012040008050) and KLGHEI (KLB11003).

REFERENCES

1. J. M. Tarascon, and M. Armand, *Nature,* **2001,** *414,* 359.
2. F. Cheng, J. Liang, Z. Tao and J. Chen, *Adv. Mater,* **2011,** *23,* 1695.
3. M. Winter, J. O. Besenhard, M. E. Spahr, and P. Novak, *Adv. Mater,* **1998,** *10,*725.
4. C. -Y. Chou, H. Kim and G. S. Hwang, *J. Phys. Chem. C,* **2011,** *115,* 20018.
5. J. Graetz, C. C. Ahn, R. Yazami and B. Fultz, *J. Electrochem. Soc,* **2004,** *151,* A698.
6. B. Wang, X. L. Li, B. Luo, J. X. Yang, X. J. Wang, Q. Song, S. Y. Chen and L. J. Zhi, *Small,* **2013,** *9,* 2399
7. H. Lee, H. Kim, S.-G. Doo and J. Cho, *J. Electrochem. Soc,* **2007,** *154,* A343.
8. G. Cui, L. Gu, L. Zhi, N. Kaskhedikar, P. A. van Aken, K. Müllen and J. Maier, *Adv. Mater,* **2008,** *20,* 3079.
9. S.-M. Paek, E. Yoo and I. Honma, *Nano Lett,* **2009,** 9, 72.
10. D.-J. Xue, S. Xin, Y. Yan, K.-C. Jiang, Y.-X. Yin, Y.-G. Guo and L.-J. Wan, *J. Am. Chem. Soc,* **2012,** *134,* 2512.
11. J. K. Lee, K. B. Smith, C. M. Hayner and H. H. Kung, *Chem. Comm,* **2010,** *46,* 2025.
12. H. Kim, Y. Son, C. Park, J. Cho and J. Choi, *Angew. Chemie int. Ed,* **2013,** *52,* 5997.
13. K. S. Novoselov, A. K. Geim, S. V. Morozov, D. Jiang, Y. Zhang, S. V. Dubonos, V. I. Grigorieva and A. A. Firsov, *Science,* **2004,** *306,* 666.
14. A. K. Geim and K. S. Novoselov, *Nat. Mater,* **2007,** *6,* 183.
15. A. Reina, X. T. Jia, J. Ho, D. Nezich, H. Son, V. Bulovic, M. S. Dresselhaus and J. Kong, *NonoLett,* **2009,** *9,* 30.
16. H. X. Zhang and P. X. Feng, *Carbon,* .**2010,** *48,* 359.
17. M. A. Pimenta, G. Dresselhaus, M. S. Dresslhaus,; L. G. Cancado, A. Jorio and R. Saito, *Phys. Chem. Chem. Phys,* .**2007,** *9,* 1276.
18. Y. Y. Wang, Z. H. Ni, Z. X. Shen, H. M. Wang and Y. H. Wu, *Appl. Phys. Lett,* **2008,** *92,* 043121.
19. A. C. Ferrari, J. C. Meyer, V. Scardaci, C. Casiraghi, M. Lazzeri, F. Mauri, S. Piscanec, D. Jiang, K. S. Novoselov, S. Roth and A. K. Geim, *Phys. Rev. Lett,* **2006,** *97,* 187401.
20. M. Zhu, L. Y. Dai, N. S. Gu, B. Cao and L. Z. Ouyang, *J. Alloys Compd,* **2009,** *478,* 624.
21. H. Liu, R. Z. Hu, M. Q. Zeng, J. W. Liu and M. Zhu, *J. Mater. Chem,* .**2012,** *22,* 8022.
22. S. A. Needham, A. Calka, G. X. Wang, A. Mosbah and H. K. Liu, *Electrochem.Commun,* **2006,** *8,* 434.
23. E. Cruz-Silva, X. Jia, H. Terrones, B. G. Sumpter, M. Terrones, M. S. Dresselhaus and V. Meunier, *ACS Nano,* **2013,** *7,* 2834.
24. S. Z. Butler, S. M. Hollen, L. Cao, Y. Cui, J. A. Gupta, H. R. Gutiérrez, T. F. Heinz, S. S. Hong, J. Huang, A. F.

Ismach, E. Johnston-Halperin, M. Kuno, V. V. Plashnitsa, R. D. Robinson, R. S. Ruoff, S. Salahuddin, J. Shan, L. Shi, M. G. Spencer, M. Terrones, W. Windl and J. E.Goldberger, *ACS Nano,* **2013,** *7,* 2898.
25. J. K. Feng, M. O. Lai and L. Lu, *Electrochim. Acta,* **2012,** 62, 103.
26. W. F. Chen, Z. Y. Zhu, S. R. Li, C. H. Chen and L. F. Yan, *Nanoscale,* **2012,** *4,* 2124.
27. N. Takami, A. Satoh, M. Hara and T. Ohsaki, *J. Electrochem. Soc,* **1995,** *142,* 371.
28. S. B. Yang, X. L. Feng and K. Müllen, *Adv. Mater,* **2011,** *23,* 3575.
29. Y. Sun, X. Hu, W. Luo and Y. Huang, *ACS Nano,* **2011,** *5,* 7100.